1-1-2014

Modeling a soft robotic mechanism articulated with dielectric elastomer actuators

Chuc H. Nguyen
University of Wollongong, chuc@uow.edu.au

Gursel Alici
University of Wollongong, gursel@uow.edu.au

Rahim Mutlu
University of Wollongong, rmutlu@uow.edu.au

Modeling a soft robotic mechanism articulated with dielectric elastomer actuators

Abstract

In this paper, a translational actuation mechanism in the form of a parallel-crank mechanism (i.e. double-crank 4-bar mechanism) articulated with two dielectric elastomer actuators working in parallel are fabricated. This structure, which is a fully soft mechanism, is established by stretching a dielectric elastomer (DE) film over a PET (polyethylene terephthalate) frame so that the energy released from the stretched DE film is stored in the frame as bending energy. The mechanism generates a translational output under a driving voltage applied between two electrodes of the DE film. The visco-elastic models are proposed for the mechanism so that the mechanical properties of the actuator can more accurately be incorporated into the mechanism model. The proposed model accurately predicts the experimental frequency response of the mechanism at different voltages.

Keywords

dielectric, elastomer, articulated, mechanism, robotic, soft, actuators, modeling

Disciplines

Engineering | Science and Technology Studies

Publication Details

Nguyen, C. Huu., Alici, G. & Mutlu, R. (2014). Modeling a soft robotic mechanism articulated with dielectric elastomer actuators. 2014 IEEE/ASME International Conference on Advanced Intelligent Mechatronics (AIM) (pp. 599-604). United States: Institute of Electrical and Electronics Engineers.

Modeling a Soft Robotic Mechanism Articulated with Dielectric Elastomer Actuators

Chuc Huu Nguyen, Gursel Alici, and Rahim Mutlu

***Abstract*— In this paper, a translational actuation mechanism in the form of a parallel-crank mechanism (i.e. double-crank 4-bar mechanism) articulated with two dielectric elastomer actuators working in parallel are fabricated. This structure, which is a fully soft mechanism, is established by stretching a dielectric elastomer (DE) film over a PET (polyethylene terephthalate) frame so that the energy released from the stretched DE film is stored in the frame as bending energy. The mechanism generates a translational output under a driving voltage applied between two electrodes of the DE film. The visco-elastic models are proposed for the mechanism so that the mechanical properties of the actuator can more accurately be incorporated into the mechanism model. The proposed model accurately predicts the experimental frequency response of the mechanism at different voltages.**

***Index Terms*— soft robotic mechanism, smart actuators, dielectric elastomer actuators.**

I. Introduction

Recent progress in electroactive polymers (EAPs) has attracted the attention of a lot of researchers [1]. Among EAP actuators, dielectric elastomer actuators (DEAs) are considered to be the most promising because of their high strain and force outputs, easy fabrication, flexibility, light weight and low cost [2], [3]. DEAs in different modes and shapes have been used for many applications including robotics and mechatronics [4-9].

A soft robotic mechanism articulated with DEAs has a wide range of applications in different fields especially in biomedical engineering, which requires programmable stiffness and flexibility that the conventional actuators are unable to provide. As an example, a self-organized minimum energy structure is able to behave like nastic structures in nature [10]. Another practical example is a binary actuator, that is a compliant diamond-shaped dielectric elastomer actuator [10]. The diamond–shaped actuator, which is able to output a bi-stable motion, can be used for medical applications in a Magnetic Resonance Imaging (MRI) system. Additionally, a linear compliant actuator whose shape is conical is fabricated using a dielectric elastomer and compliant frame [11]. This mechanism can generate a mono-directional or bidirectional movement. As an extension of this linear actuator a six degree of freedom conical DEAs is established to produce rotational actuation outputs which can be exploited in minimally invasive medical devices [12]. Those proposed mechanisms, which are flexible and have a high energy density, show promising properties in various applications. However, these mechanisms are based on complex structures. This prevents them from biomedical applications which require a simple and monolithic mechanism. Therefore, in this paper, we go a further step to propose a flexible parallel mechanism using minimum energy mechanism shown in [13]. This basic soft mechanism can generate a translational movement. The proposed mechanism includes two bending actuators or cranks and a soft (Polyethylene terephthalate) bar—it is a fully soft robotic mechanism. This mechanism is articulated by a pair of bending actuators replicating the articulation of cranks in the corresponding conventional mechanism. The proposed mechanism can generate a translational movement and a compliant force output which are essential for human-machine interactions in frontier biomedical applications.

The elastic modulus of the DEAs is not constant and changes during operation, due to the viscoelastic properties of the DE material [3]. These properties must be considered in modeling the DEAs and a mechanism articulated with the actuators. Therefore, we have experimentally identified a set of transfer function models in order to accurately predict the position response of the mechanism for a wide range of frequencies and driving voltages. Additionally, the relationship between the displacement output and driving voltage is identified by a non-linear least square estimation method.

The remainder of this paper is organized as follows. In Section II, we introduce the proposed mechanism and the bending actuators based on the minimum energy principle. Modeling and analysis concepts for the actuators and mechanism are provided in Section III. We have provided the experimental frequency response results and the identified transfer function models in Section IV. Conclusions and future work are reported in Section V.

II. The Proposed Mechanism

A. The operation principle of dielectric elastomer actuators

The operating principle of a dielectric elastomer actuator is shown in Fig. 1, where compliant electrodes are applied on both sides of the dielectric material. When an electrical stimulus is applied to the electrodes, the Maxwell stress

* This work was supported by research funds in Intelligent Nano-Tera Systems Research Laboratory of University of Wollongong.

R. Mutlu and G. Alici (corresponding author) are with the School of Mechanical, Materials and Mechatronic Engineering and ARC Centre of Excellence for Electromaterials, University of Wollongong, Australia (e-mail: gursel@uow.edu.au, rmutlu@uow.edu.au)

C. H. Nguyen is with Hue Industrial College, VietNam and the School of Mechanical, Materials and Mechatronic Engineering University of Wollongong, Australia (Email: chucnh@gmail.com).

deforms the dielectric elastomer and generates the lateral displacement which is the mechanical output of the actuator. It is this mechanical output which is exploited to design various actuation configurations in order to generate the desired output.

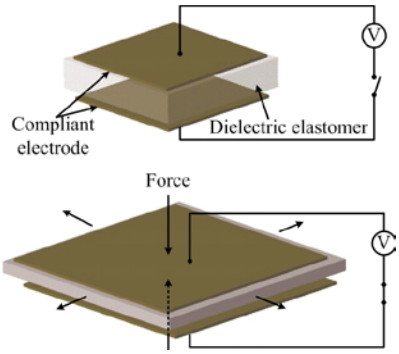

Fig. 1. Operation principle of dielectric elastomer actuators [5]. .

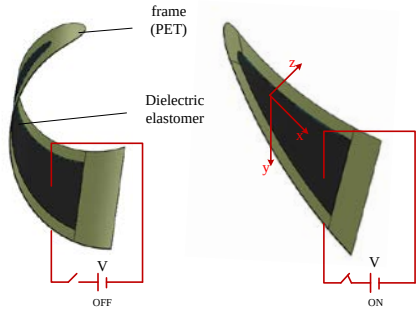

Fig. 2. The working principle of the bending actuator built as a minimum energy structure. The wider end of the structure is fixed to generate the bending motion.

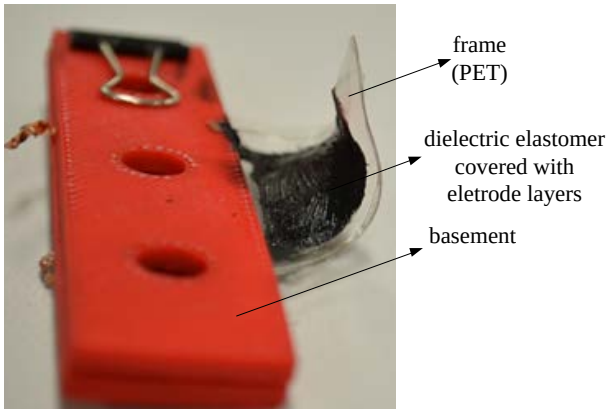

Fig. 3. The bending actuator based on the minimum energy principle.

B. *Description of bending actuator*

In this section, a bending mechanism based on dielectric elastomer, like a cantilever beam in deflection is described. To this aim, we have exploited the minimum energy principle (MEP) [13] to build the bending actuator, which is made of a DE film stretched over a PET (Polyethylene terephthalate) frame. The DE is covered with electrodes on both sides and attached to the frame (PET). The working principle of this minimum energy structure which acts like a bending actuator is shown in Fig. 2 and Fig.3. In addition, the outline of the mechanism is described in Fig. 4. When a driving voltage is applied, the film compresses in the thickness direction and expands in the lateral direction. The expansion of the film releases the energy stored in the PET frame. Consequently, the bending angle of this mechanism depends on the driving voltage

C. *Parallel-crank mechanism articulated*

A parallel-crank four-bar mechanism is designed to demonstrate the efficacy of a bending actuator based on the minimum energy principle in generating a translational output. In addition, thanks to their compliance, this mechanism can be applied in biomedical applications that require compliance matching or soft-on-soft contact. The proposed mechanism is shown in Fig. 4. The mechanism consists of two bending actuators (two dielectric elastomer actuators) acting like two flexural joints that can actuate by themselves, as shown in Fig. 5. When the driving voltage is applied through two electrodes of the actuator, the mechanism will bend from the initial position, θ_0 to the final position θ.

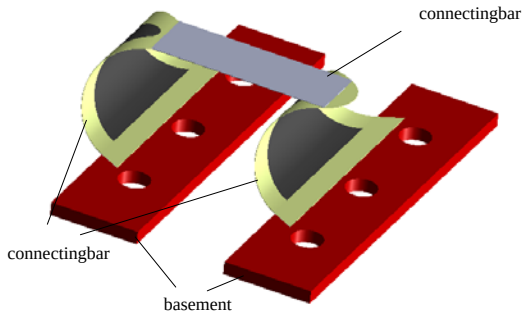

Fig. 4. The proposed parallel mechanism.

III. MODELING OF MECHANISM

A. *Analysis of bending actuator*

When the driving voltage is applied to the DE film, the Maxwell stress is generated [2], as expressed below:

$$\sigma_z = \varepsilon_r \varepsilon_0 \left(\frac{V}{t_d} \right)^2 \quad (1)$$

where σ_z is the Maxwell stress, and ε_r, ε_0 are the free-space permittivity ($8.85\times10^{-12}\ F/m$) and the dielectric constant of the material, respectively. V is the driving voltage applied between the electrodes of the DE film. t_d is the thickness of the film.

Assuming that the DE film expands in the x-direction , as shown in Fig. 3. The strain of the film in the x-direction is given by:

$$\varepsilon_x = \frac{\nu\sigma_z}{E_d} = \frac{\nu\varepsilon_r\varepsilon_0\left(\frac{V}{t_d}\right)^2}{E_d} \quad (2)$$

where E_d is the elastic modulus of the DE film. ν is Poisson's ratio.

The curvature of the composite minimum energy bending actuator changes due to the expansion of the film under an applied voltage. This change in the curvature of each bending actuator is given as follows [14, 15]:

$$\kappa = \frac{1}{R_0} - \frac{1}{R} = \frac{\varepsilon_x}{\frac{t_f + t_d}{2} + \frac{2\left(E_d I_d + E_f I_f\right)}{t_d + t_f}\left(\frac{1}{E_d A_d} + \frac{1}{E_f A_f}\right)} \quad (3)$$

where R_0 is the initial radius of curvature of the actuator. t_f, E_f are the thickness and elastic modulus of the PET frame, respectively. A_d and A_f are the areas of the DE film and PET frame, respectively. I_d and I_f are the area moment of inertias of the DE film and PET frame, respectively.

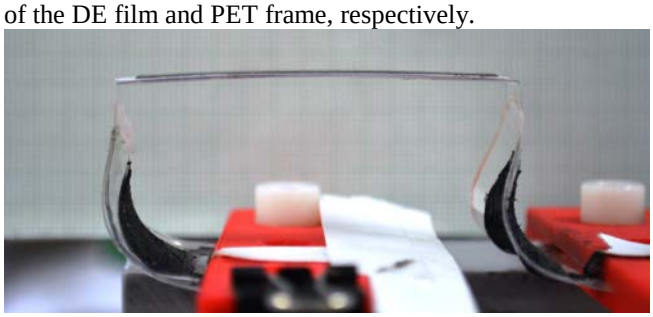

(a)

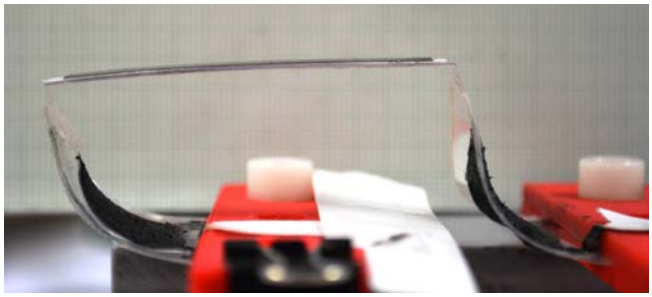

(b)

Fig. 5. The parallel-crank mechanism (a) initial state (b) bending state under a voltage input.

By incorporating Eq.2 into Eq.3, the following transfer function of curvature of bending actuator can be obtained as:

$$G_b(s) = \frac{\frac{1}{R_0} - \frac{1}{R}}{V^2} = \frac{\nu\varepsilon_r\varepsilon_o / \left(E_d t_d^{\,2}\right)}{\frac{t_f + t_d}{2} + \frac{2\left(E_d I_d + E_f I_f\right)}{t_d + t_f}\left(\frac{1}{E_d A_d} + \frac{1}{E_f A_f}\right)} \quad (4)$$

A viscoelastic behavior of the DE film is incorporated into the actuator model in order to accurately consider the change in the elastic modulus. We employ the Standard Linear Solid model to describe the visco-elastic behaviour of the film. The proposed model is described in Fig. 6 (a).

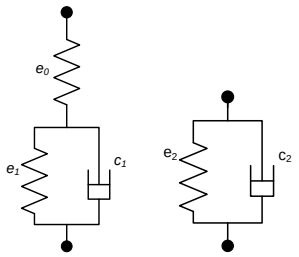

(a) (b)

Fig. 6. The viscoelastic model of the DE film (a) and the PET frame (b).

With reference to Fig.6 (a), we obtain the effective modulus of elasticity of the DE film as follows:

$$\frac{1}{E_d} = \frac{1}{e_0} + \frac{1}{e_1 + c_1 s} \quad (5)$$

where e_0 indicates the modulus of elasticity of the dielectric elastomer layer under an instantaneous strain, e_1 and c_1 are the modulus of elasticity and viscosity of the DE layers, respectively, due to the maximum retarded strain and the rate of strain after the instantaneous strain region in the creep curve [4].

The viscoelastic behavior of the PET frame can be expressed by the Kelvin Voigt model [16], as shown in Fig. 6 (b). The effective modulus of elasticity of the frame is derived as follows:

$$E_f = e_2 + c_2 s \quad (6)$$

where e_2, c_2 are the elastic modulus and damping ratio of the frame, respectively. Incorporating Eqs. (5) and (6), into Eq. 4 results in the following transfer function $G_b(s)$:

$$G_b(s) = \frac{b_3 s^3 + b_2 s^2 + b_1 s + b_0}{a_4 s^4 + a_3 s^3 + a_2 s^2 + a_1 s + a_0} \quad (7)$$

where a_i ($i = 0..4$) and b_i ($i = 0..3$) are the parameters based on the mechanical and viscoelastic properties of the actuators. The details of how these parameters are provided in Appendix A.

B. *Analysis of the parallel mechanism*

The schematic of the parallel-crank mechanism is shown in Fig.7. When the driving voltage is applied, the connecting bar moves a distance, *d*, in the vertical direction:

$$d = L\sin(\theta) - L_0\sin(\theta_0) \tag{8}$$

where L_0 and θ_0 are the initial length and bending angle of each actuator, respectively. Similarly, L and θ are the final length and bending angle, respectively, upon the application of a voltage. For a conventional mechanism made of rigid links and joints, L and L_0 are equal to each other. For the compliant four-bar mechanism we built, however, they are not equal to each other. This is because the parallelogram topology we have used does not cause any change in the parallel orientation of the coupling bar.

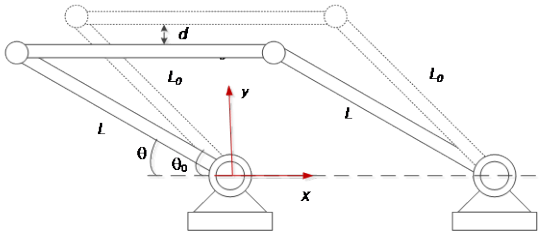

Fig. 7. Schematic of the parallel mechanism from a non-actuated configuration to an actuated configuration.

As shown in Fig. 8, R_0 are R are the initial curvature and final curvatures of the bending actuators, respectively. The lengths L and L_0 are obtained as follows:

$$\begin{aligned} L_0 &= 2R_0\sin\theta_0 \\ L &= 2R\sin\theta \end{aligned} \tag{9}$$

Incorporating Eq.9 into Eq.8 results in:

$$\begin{aligned} d &= 2R_0\sin\theta_0\sin\theta_0 - 2R\sin\theta\sin\theta \\ &= (R_0 - R) - (R_0\cos 2\theta_0 - R\cos 2\theta) \end{aligned} \tag{10}$$

We use the following Taylor series of expansions to simplify Eq.10:

$$\begin{aligned} \cos 2\theta_0 &\approx 1 - \frac{4\theta_0^2}{2} \\ \cos 2\theta &\approx 1 - \frac{4\theta^2}{2} \end{aligned} \tag{11}$$

By incorporating Eq. 11 into Eq.10, the linear movement of the coupling bar is obtained as follows:

$$d = 2\left(R_0\,\theta_0^2 - R\,\theta^2\right) \tag{12}$$

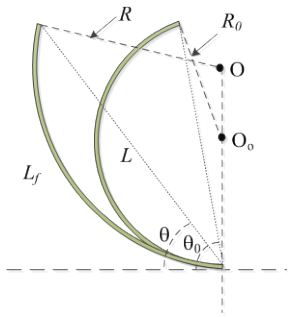

Fig. 8. Schematic of each bending actuator at their initial and final configurations.

The geometric relationships between the angular position and the radius curvature of the bending actuator shown in Fig. 8 are obtained as follows:

$$\theta_0 = \frac{L_f}{2R_0} \tag{13}$$

$$\theta = \frac{L_f}{2R} \tag{14}$$

where L_f is the length of the PET frame of the bending actuator.

By combining Eqs. (12), (13) and (14), the linear distance, *d*, is expressed as follows:

$$d = \frac{L_f^{\,2}}{2}\left(\frac{1}{R_0} - \frac{1}{R}\right) \tag{15}$$

From Eqs. (4) and (15), we obtain the following relationship between the output 'd' and the square of the applied voltage:

$$G(s) = \frac{d}{V^2} = \frac{L_f^2}{2}\frac{\frac{1}{R_0} - \frac{1}{R}}{V^2} = \frac{L_f^2}{2}G_b(s) \tag{16}$$

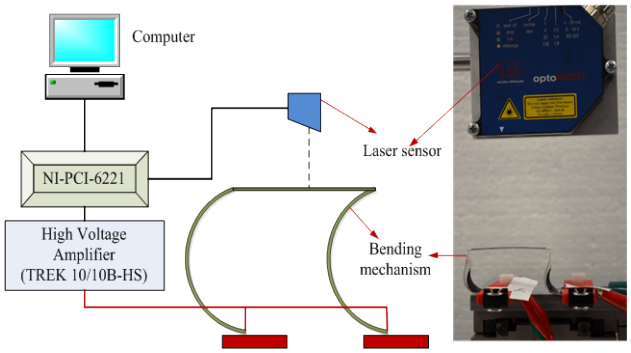

Fig. 9. The experimental setup.

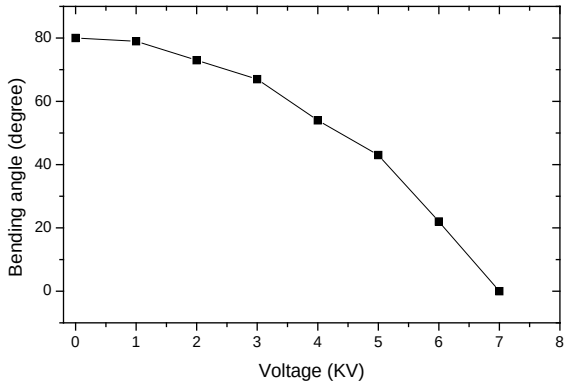

Fig. 10. The relationship between the bending angle and the input voltage of bending actuator (θ).

I. Experimental Set-up and Model Identification

The minimum energy bending actuators are fabricated from VHB 4905, from 3M Inc. Two sides of this film were covered with conductive carbon grease. The experimental set-up depicted in Fig. 9 is employed to activate the mechanism and measure its displacement output '*d*' via a laser displacement sensor (ILD 1700-50) from Micro-Epsilon Inc. A high voltage amplifier (10/10B-HS) from TREK Inc. was used to amplify the driving voltage, which was varied from 0 KV to 7KV to obtain the experimental relationship between the displacement (i.e. bending angle) output and the driving voltage, as shown in Fig.10.

Moreover, the output displacement '*d*' was experimentally measured as a function of the input voltage, as shown in Fig. 11, which indicates that the displacement '*d*' is proportional to the square of the voltage up to *3 KV*. When the voltage is larger than *3 KV*, this relationship does not hold. We have, therefore, divided this displacement output into 3 ranges; (i) 0<V≤3.0 KV, (ii) 3.0KV<V≤4.0KV and (iii) 4.0KV<V≤5.0 KV.

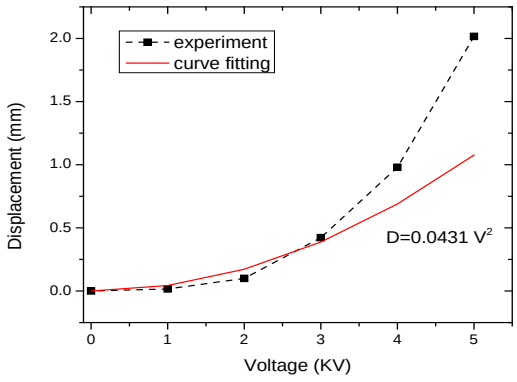

Fig. 11. The nonlinear relationship between the displacement output and the driving voltage in steady state.

The experimental frequency responses between the displacement output and square of the voltage input were obtained for these three ranges and are shown in Fig. 12. The dynamic response of the mechanism changes with the input voltage due to the viscoelastic properties and non-linearities associated with the silicone-based DE material used [17].

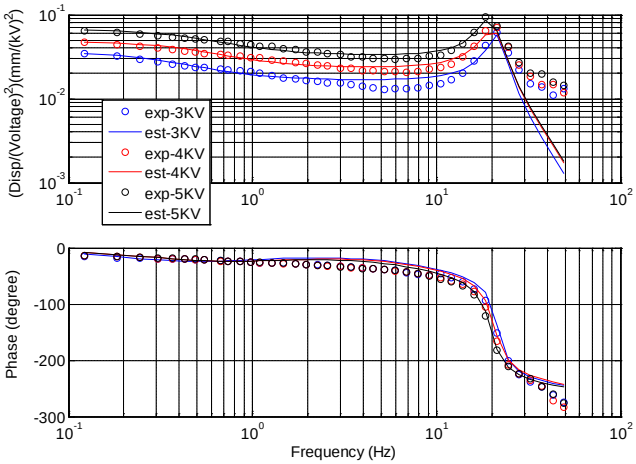

Fig. 12. Experimental and estimated frequency responses of the parallel-crank mechanism at different voltages.

Three transfer functions corresponding to the experimental data in Fig. 122 are experimentally identified, and shown in

Table 1. The transfer functions $G_1(s)$, $G_2(s)$ and $G_3(s)$ describe the response of the mechanism at *3 KV*, 4 *KV* and 5 *KV*, respectively. The order of these transfer functions is the same as that of the transfer function in Eq.7.

Table 1. The transfer function models of the proposed mechanism for different voltage ranges.

V (KV)	Transfer function
3	$G_1(s) = \dfrac{0.01s^3 + 0.01s^2 + 135.7s + 96.11}{s^4 + 22.17s^3 + 536.1s^2 + 8327s + 2636}$
4	$G_2(s) = \dfrac{0.01s^3 + 0.01s^2 + 184.9s + 179.7}{s^4 + 24.26s^3 + 524.7s^2 + 8229s + 3663}$
5	$G_3(s) = \dfrac{0.01s^3 + 0.01s^2 + 1007s + 1046}{s^4 + 20.04s^3 + 460.9s^2 + 6070s + 2685}$

II. Conclusions

This study has proposed a new linear actuation mechanism articulated with DE bending actuators based on the minimum energy principle. This is the first time that DEAs have been tested while articulating a mechanism which converts a bending displacement into a translational displacement effectively. The transfer function models of the mechanism were experimentally identified. The model takes into account the viscoelastic properties of the dielectric film in order to describe the mechanical behaviour of the actuator for a range of driving voltages. The experimental and theoretical results

indicate that the proposed model is accurate enough to predict the displacement output of the mechanism.

Future work involves (i) quantifying the feasibility of inversion-based control strategies for such actuators, (ii) undertaking the design optimization of the mechanism to achieve a more accurate displacement output from the coupling link, and (iii) evaluating its compliance limits while maintaining the parallel configuration of its coupling link.

APPENDIX A: COEFFICIENTS OF THE TRANSFER FUNCTION IN EQ.7

For

$$C = \upsilon \varepsilon_r \varepsilon_0 / t_d^{\,2} \tag{17}$$

$$H = \frac{1}{2}\left(h_p + h_f\right) \tag{18}$$

the parameters b_i ($i=1,2,3$) of Eq. (7) are obtained as follows:

$$b_0 = H\,C\,A_p A_f \left(e_2 e_0^{\,2} + 2e_2 e_0 e_1 + e_2 e_1^{\,2}\right) \tag{19}$$

$$\begin{aligned} b_1 = {} & H\,C\,A_p A_f \,(c_2 e_0^{\,2} + 2c_2 e_0 e_1 + 2c_1 e_2 e_0 \\ & + c_2 e_1^{\,2} + 2c_1 e_2 e_1) \end{aligned} \tag{20}$$

$$b_2 = H\,C\,A_p A_f \,(c_1^{\,2} e_2 + 2c_1 c_2 e_0 + 2c_1 c_2 e_1) \tag{21}$$

$$b_3 = H\,C\,A_p A_f c_1^{\,2} c_2 \tag{22}$$

The parameters a_i ($i=1,2,3,4$) of Eq. (7) are similarly obtained as follows:

$$\begin{aligned} a_0 = {} & A_f I_f e_0^2 e_2^2 + A_f I_f e_1^2 e_2^2 + A_p I_p e_0^2 e_1^2 + 2A_f I_f e_0 e_1 e_2^2 \\ & + A_f I_p e_0 e_1^2 e_2 + A_f I_p e_0^2 e_1 e_2 + A_p I_f e_0 e_1^2 e_2 \\ & + A_p I_f e_0^2 e_1 e_2 + A_f A_p H^2 e_0 e_1^2 e_2 + A_f A_p H^2 e_0^2 e_1 e_2 \end{aligned} \tag{23}$$

$$\begin{aligned} a_1 = {} & 2A_f I_f c_1 e_0 e_2^2 + 2A_f I_f c_1 e_1 e_2^2 + 2A_f I_f c_2 e_0^2 e_2 \\ & + 2A_f I_f c_2 e_1^2 e_2 + A_f I_p c_1 e_0^2 e_2 + A_f I_p c_2 e_0 e_1^2 \\ & + A_f I_p c_2 e_0^2 e_1 + A_p I_f c_1 e_0^2 e_2 + A_p I_f c_2 e_0 e_1^2 \\ & + A_p I_f c_2 e_0^2 e_1 + 2A_p I_p c_1 e_0^2 e_1 + A_f A_p H^2 c_1 e_0^2 e_2 \\ & + A_f A_p H^2 c_2 e_0 e_1^2 + A_f A_p H^2 c_2 e_0^2 e_1 \\ & + 4A_f I_f c_2 e_0 e_1 e_2 + 2A_f I_p c_1 e_0 e_1 e_2 \\ & + 2A_p I_f c_1 e_0 e_1 e_2 + 2A_f A_p H^2 c_1 e_0 e_1 e_2 \end{aligned} \tag{24}$$

$$\begin{aligned} a_2 = {} & A_f I_f c_2^2 e_0^2 + A_f I_f c_1^2 e_2^2 + A_f I_f c_2^2 e_1^2 + A_p I_p c_1^2 e_0^2 \\ & + A_f I_p c_1 c_2 e_0^2 + A_p I_f c_1 c_2 e_0^2 + 2A_f I_f c_2^2 e_0 e_1 \\ & + A_f I_p c_1^2 e_0 e_2 + A_p I_f c_1^2 e_0 e_2 + A_f A_p H^2 c_1 c_2 e_0^2 \\ & A_f A_p H^2 c_1^2 e_0 e_2 + 4A_f I_f c_1 c_2 e_0 e_2 + 4A_f I_f c_1 c_2 e_1 e_2 \\ & + 2A_f I_p c_1 c_2 e_0 e_1 + 2A_p I_f c_1 c_2 e_0 e_1 \\ & + 2A_f A_p H^2 c_1 c_2 e_0 e_1 \end{aligned} \tag{25}$$

$$\begin{aligned} a_3 = {} & 2A_f I_f c_1 c_2^2 e_0 + 2A_f I_f c_1 c_2^2 e_1 + 2A_f I_f c_1^2 c_2 e_2 \\ & + A_f I_p c_1^2 c_2 e_0 + A_p I_f c_1^2 c_2 e_0 + A_f A_p H^2 c_1^2 c_2 e_0 \end{aligned} \tag{26}$$

$$a_4 = A_f I_f c_1^2 c_2^2 \tag{27}$$

REFERENCES

[1] Y. Bar-Cohen, *Electroactive Polymer (EAP) Actuators as Artificial Muscles: Reality, Potential, and Challenges*, Second ed., 2004.

[2] R. Pelrine, R. Kornbluh, Q. Pei, and J. Joseph, "High-Speed Electrically Actuated Elastomers with Strain Greater Than 100%," *Science*, vol. 287, pp. 836-839, 2000.

[3] P. Brochu and Q. Pei, "Advances in Dielectric Elastomers for Actuators and Artificial Muscles," *Macromolecular Rapid Communications*, vol. 31, pp. 10-36, 2010.

[4] N. H. Chuc, J. C. Koo, Y. K. Lee, J. Nam, and H. R. Choi, "Artificial muscle actuator based on the synthetic elastomer," *Int. J. Control Autom. Syst*, vol. 6, pp. 894-903, 2008.

[5] C. H. Nguyen, N. H. L. Vuong, *D.* S. Kim, H. P. Moon, J. C. Koo, L. Young Kwan, *et al.*, "Fabrication and Control of Rectilinear Artificial Muscle Actuator," *IEEE/ASME Transactions on Mechatronics*, vol. 16, pp. 167-176, 2011.

[6] H. R. Choi, K. Jung, S. Ryew, J.-D. Nam, J. JaeWook, J. C. Koo, *et al.*, "Biomimetic soft actuator: design, modeling, control, and applications," *IEEE/ASME Transactions on Mechatronics*, vol. 10, pp. 581-593, 2005.

[7] G. Kovacs, L. Düring, S. Michel, and G. Terrasi, "Stacked dielectric elastomer actuator for tensile force transmission," *Sensors and Actuators A: Physical*, vol. 155, pp. 299-307, 2009.

[8] K. K. Ahn, D. Q. Truong, D. N. C. Nam, J. I. Yoon, and S. Yokota, "Position control of ionic polymer metal composite actuator using quantitative feedback theory," *Sensors and Actuators A: Physical*, vol. 159, pp. 204-212, 2010.

[9] X. Wang, G. Alici, and C. H. Nguyen, "Adaptive sliding mode control of tri-layer conjugated polymer actuators," *Smart Materials and Structures*, vol. 22, p. 025004, 2013.

[10] J. S. Plante, "Dielectric Elastomer Actuators for Binary Robotics and Mechatronics," Doctor of Philosophy, Mechanical Engineering, Massachusetts Institute of Technology, 2006.

[11] G. Berselli, R. Vertechy, G. Vassura, and V. Parenti-Castelli, "Optimal Synthesis of Conically Shaped Dielectric Elastomer Linear Actuators: Design Methodology and Experimental Validation," *Mechatronics, IEEE/ASME Transactions on*, vol. 16, pp. 67-79, 2011.

[12] A. T. Conn and J. Rossiter, "Towards holonomic electro-elastomer actuators with six degrees of freedom," *Smart Materials and Structures*, vol. 21, p. 035012, 2012.

[13] G. Kofod, M. Paajanen, and S. Bauer, "Self-organized minimum-energy structures for dielectric elastomer actuators," *Applied Physics A*, vol. 85, pp. 141-143, 2006/11/01 2006.

[14] M. J. Smith, "A parameter identification study of frequency response data for a tri-layered conjugated polymer actuator displacement model," Undergraduate thesis, University of Wollongong, 2012.

[15] E. D. Blanchard, M. J. Smith, and C. H. Nguyen, "Parameter identification study of frequency response data for a trilayer conjugated polymer actuator displacement model," in *Advanced Intelligent*

Mechatronics (AIM), 2013 IEEE/ASME International Conference on, 2013, pp. 1102-1107.

[16] N. M. Alves, J. L. G. Ribelles, and J. F. Mano, "Study of the viscoelastic properties of PET by thermally stimulated recovery," *Plastics, Rubber and Composites* vol. 32, pp. 281-290, 2003.

[17] K. Jung, J. Lee, M. Cho, J. C. Koo, J.-d. Nam, Y. Lee, *et al.*, "Development of enhanced synthetic elastomer for energy-efficient polymer actuators," *Smart Materials and Structures*, vol. 16, p. S288, 2007.